Renewable Energy and Power Quality Journal
https://repqj.com/index.php/repqj/index
RE&PQJ, Vol. 23, No. 5, 2025

Stability Analysis Based on Hybrid αβ-impedance Model of Grid-Connected Inverters under Weak Grid

Jun Gu[1,2], Tianle Li[1,2], Jing Shen[1,2], Hao Ma[1,2], Meiying Yang[1,2]

[1]State Grid Beijing Electric Power Research, Beijing (China)
[2]Beijing Dingcheng Hong'an Technology Development Co., Ltd, Beijing (China)
[*]Corresponding author email: gujun@bj.sgcc.com.cn

Abstract. The robustness of the grid-connected inverter (GCI) system in weak grids is deteriorated due to consider discrete characteristics of the GCI control system. Under the same main circuit parameters and control loop parameters, the small signal models of the GCI controlled with continuous $\alpha\beta$ -impedance model and hybrid $\alpha\beta$ -impedance model are constructed, respectively. Compared with the small-signal hybrid impedance model of the GCI controlled in dq domain, the number of control loops of GCI controlled in $\alpha\beta$ domain is one less. Moreover, the rationale behind the enhanced stability of the GCI system governed by a hybrid $\alpha\beta$ -impedance control scheme, as compared to one based on hybrid dq -impedance control, is examined and elucidated. This lays a theoretical underpinning for the analysis and development of a discretized control loop to enhance the stability of the GCI under weak grid. Finally, the theoretical analysis is confirmed through simulation and experimental validations.

Key words. Grid-connected Inverter (GCI), Hybrid Impedance Model, Weak Grid, Stability Margin

1. Introduction

Recently, the swift and substantial growth in renewable energy sources, particularly wind and photovoltaic power generation, has spurred intense interest and concern regarding the stability and robustness of grid-connected inverter (GCI) systems [1], [2]. As these systems play a critical role in integrating renewable energy into the grid, ensuring their stability has become a paramount issue within the energy industry [3,4]. Moreover, the GCI often serve as a critical interface between renewable energy sources and the grid [5,6]. When GCI is connected to a weak grid, the presence of grid impedance and the influence of phase-locked loop (PLL) bandwidth will make the dynamic performance of the control system more complex, and stability problems of the GCI increasingly prominent [7], [8]. Based on this, the stability analysis approach of impedance modeling has become an important method for GCI system stability analysis [9,10].

Significant scholarly contributions have been made in the field of impedance-based modeling and stability analysis for grid-connected inverter systems. According to impedance modeling, the coordinate conversion mode can be divided into two categories: 1) in the $\alpha\beta$ domain or the stationary reference frame: 2) in the synchronous rotation coordinate system of the dq domain.

In [11], the dq -impedance model of GCI system with considering the PLL influence is constructed, and the key factors influencing of system stability are analyzed. The construction of sequence impedance models for GCI in the synchronous reference frame is detailed, with emphasis on the decoupling of the positive and negative sequence subsystems, as described in [12]. A single-input single-output (SISO) framework is put forth [13] to illustrate the interaction between the phase-locked loop (PLL) and the controller of the GCI system with respect to grid synchronization. By establishing a 3x3 dq -impedance model in [14], that includes AC side impedance information, DC side impedance information, and AC/DC side coupling impedance information. the specific operating status of VSC in weak grids can be more accurately predicted. The works in [15], a simple dq -impedance extension method is proposed and considers all unbalance factors to derive the impedance model of the converter. The linear active interference suppression controller is applied to the PLL, the ability to suppress oscillation instability of the system is enhanced [16,17]. In [18], the PLL is improved by adding a second-order filter to reduce the negative effects of frequency coupling, thereby improving the stability of system operation. The works in [19], small-signal models for GCI control are developed in both dq domains and $\alpha\beta$ domains, which reveals

the stability of GCI controlled in $\alpha\beta$ domain is superior to in dq domain.

The studies mentioned above failed to account for the discrete nature of the control systems during the sampling process. All aspects of the system are considered as continuous-time models. However, it should be noted that GCI typically employ discrete digital control modes, making them hybrid systems [20]. As most traditional modeling methods fail to account for the discrete features of system, their stability results are often inaccurate. Moreover, it should be highlighted that there is a notable discrepancy in the phase margin (PM) once the discrete attributes of the GCI system are considered [21]. The work in [22], a technique for high-frequency impedance modeling of multiple variables is introduced, aiming to precisely capture frequencies exceeding the inverter's control bandwidth. This approach employs a pure discrete model to formulate the inverter's output admittance, along with a discussion on designing LCL filter parameters [23]. The modeling process becomes intricate due to the retention of impractical infinite series. Additionally, a GCI discrete-time current control strategy is proposed in [24], demonstrating adaptability to varying test parameters. An enhanced damping analysis approach is put forward in [25] to optimally achieve the maximum damping potential of GCI. Furthermore, [26] introduces a discrete-time model based on a wind turbine emulator, proposing an inertia compensation method focused on anticipated deviation suppression. However, frequency-domain stability analysis and verification of the established discrete-time models were not conducted. The works in [27] offers a stability assessment method based on SISO hybrid dq -impedance model norm. However, it may still provide a stable assessment for an unstable system.

To address above-mentioned challenges, a SISO hybrid $\alpha\beta$ -impedance model is proposed to analyze system stability in the article. Firstly, the hybrid $\alpha\beta$ -impedance model is derived with considering the discrete characteristics. Based on thus, the stability is assessed through changing line impedance parameters and PLL bandwidth. The analysis results are verified by theoretical analysis and experimental. Compared to the hybrid dq -impedance model in [27], the proposed hybrid $\alpha\beta$ -impedance model is simplified control process and exhibits lower conservatism. The same time, this implies that in the discrete-time domain for stability analysis provides a more accurate assessment of the GCI system's oscillatory instability.

2. Establish $\alpha\beta$ -Impedance Model of GCI System

To analyze and compare the stability of the GCI control system with modeling in continuous-time and discrete-time domains, in first, the SISO both continuous and hybrid impedance models are established in $\alpha\beta$ coordinate system. Then the systems stability is compared and analyzed by Bode diagram.

Figure 1 depicts the typical structure of the GCI system within the $\alpha\beta$ coordinate framework.

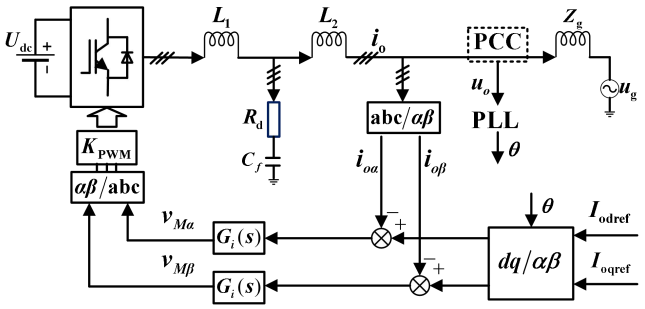

Figure 1. Typical structure diagram of GCI system

Where U_{dc} is DC-side voltage, the GCI is equipped with an LCL filter (L_1, C_f and L_2) and an AC-side damping resistor (R_d). PCC voltage (u_o), grid-connected current (i_o), grid voltage (u_g), grid impedance (Z_g), I_{odref} and I_{oqref} denote the respective d-axis and q-axis components of the reference current for the grid-connected system. $G_i(s)$ is the current PI controller; $V_{M\alpha\beta}$ is the modulation signal output, the phase angle is tracked using a SRF-PLL.

A. Establish the SISO Continuous Impedance Model

According to Figure 1, the fundamental mathematical model of GCI in the $\alpha\beta$ domain can be obtained, as depicted in Figure 2.

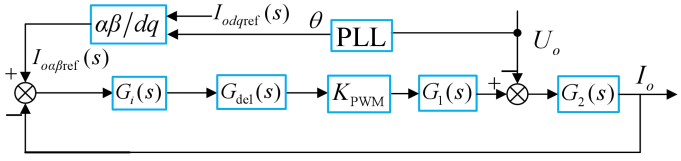

Figure 2. Fundamental mathematical model of GCI

The output current $I_o(s)$ of the GCI, as depicted in Figure 2, can be expressed as:

$$I_o(s)=\frac{J(s)}{1+J(s)}I_{oref}(s)-\frac{G_2(s)}{1+J(s)}U_o(s) \quad (1)$$

where $J(s)=G_2(s)G_1(s)K_{PWM}G_{del}(s)G_i(s)$, $Z_{L1}=sL_1$, $Z_{L2}=sL_2$, $Z_{Cf}=R_d+\frac{1}{C_f}$, then the expression of $G_1(s)$,$G_2(s)$ and $G_{del}(s)$ are

$$\begin{cases} G_1(s)=\dfrac{Z_{C_f}}{Z_{L1}+Z_{C_f}} \\ G_2(s)=\dfrac{Z_{L1}+Z_{C_f}}{Z_{L1}Z_{L2}+Z_{L2}Z_{C_f}+Z_{L1}Z_{C_f}} \\ G_{del}(s)=\mathrm{e}^{-1.5(s-j\omega_1)T_s} \end{cases} \quad (2)$$

Taking into account the negative effects caused by PLL [10], the transfer function between the grid voltage disturbance $\Delta u_o(s)$ and the grid current disturbance $\Delta i_{oref}(s)$ can be obtained

$$G_{\mathrm{PLL}}(s)=\frac{\Delta i_{\mathrm{oref}}(s)}{\Delta u_o(s)} =\frac{1}{2}\frac{k_{\mathrm{p\text{-}p11}}(s-j\omega_1)+k_{\mathrm{i\text{-}p11}}}{(s-j\omega_1)^2+U_{\mathrm{m0}}\left[k_{\mathrm{p\text{-}p11}}(s-j\omega_1)+k_{\mathrm{i\text{-}p11}}\right]} \tag{3}$$

Drawing from the previous discussion, Figure 3 depicts the small-signal impedance model of the GCI system, which includes the influence of the PLL [28].

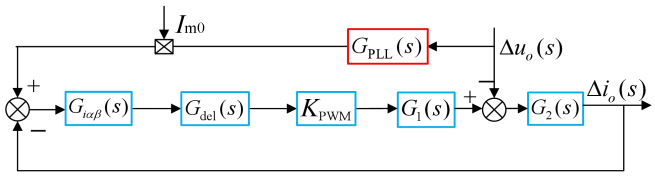

Figure 3. The small-signal impedance model of GCI system

Combining (1) and Figure 3, $\Delta i_o(s)$ can be obtained as follows:

$$\Delta i_o(s)=\frac{J(s)I_{\mathrm{m0}}G_{\mathrm{PLL}}(s)}{1+J(s)}\Delta u_o(s) -\frac{G_2(s)}{1+J(s)}\Delta u_o(s) \tag{4}$$

where I_{m0} represents the amplitude of the grid rated current.

Figure 4 illustrates the Norton equivalent circuit of the GCI system, which is derived by integrating the mathematical expressions from (4) with the detailed impedance model shown in Figure 3.

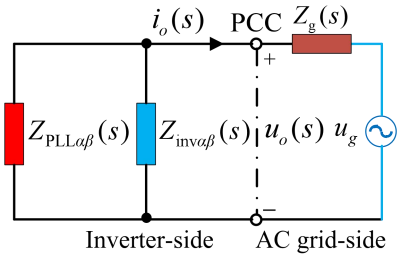

Figure 4. Norton equivalent circuit of GCI

where $Z_{\mathrm{PLL}\alpha\beta}(s)$ and $Z_{\mathrm{inv}\alpha\beta}(s)$ are

$$\begin{cases} Z_{\mathrm{PLL}\alpha\beta}(s)=-\dfrac{1+J(s)}{J(s)\mathrm{I}_{\mathrm{m0}}G_{\mathrm{PLL}}(s)} \\ Z_{\mathrm{inv}\alpha\beta}(s)=\dfrac{1+J(s)}{G_2(s)} \end{cases} \tag{5}$$

Then the SISO continuous impedance model $Z_{o\alpha\beta}(s)$ is

$$Z_{o\alpha\beta}(s)=\frac{1}{\dfrac{1}{Z_{\mathrm{PLL}\alpha\beta}(s)}+\dfrac{1}{Z_{\mathrm{inv}\alpha\beta}(s)}} \tag{6}$$

B. Establish the SISO Mixed Impedance Model

In section 2.A, all stages are treated as continuous model, which has a certain deviation on the analysis results of system stability. Therefore, accounting for the system discrete characteristics and establishing its hybrid impedance model are the work of this section.

Mathematical model of GCI hybrid system is shown in Fig.5. U_o and I_o are the continuous voltage and current outputs signals of the inverter. After a sampling process with T_s, digital signals U_o^* and I_o^* are obtained and sent to the digital controller for processing. Given that the higher-order harmonics resulting from the switching process can be considered negligible, the modulating signal produced by the digital controller is converted into the real inverter port voltage through the action of a zero-order hold (ZOH). Where '*' indicates the sampling process. In other words, the corresponding voltage and current signals or the controller transfer function are discretized.

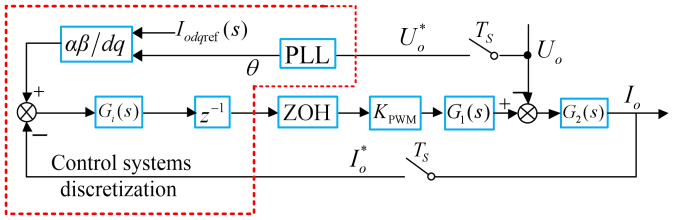

Figure 5. Block diagram of GCI mixed system

After considering the sampling process, Figure 5 can be represented by SISO hybrid small-signal model as shown in Figure 6. It is worth noting that, in comparison to the small-signal hybrid impedance model of the system in the *dq* domain, in the $\alpha\beta$ domain has one less control loop [13].

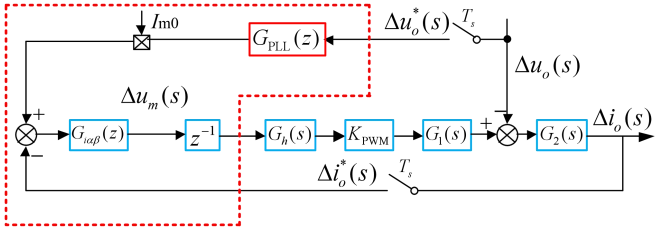

Figure 6. SISO hybrid small-signal impedance model of GCI

From Figure 6, it can be obtained:

$$\begin{cases}\Delta u_m = G_{i\alpha\beta}(z)\left[\mathrm{I_{m0}}\, G_{\mathrm{PLL}}(z)\Delta u_o^* - \Delta i_o^*\right] \\ \Delta i_o = G_2(s)\left[G_1(s)G_h(s)z^{-1}K_{\mathrm{PWM}}\Delta u_m - \Delta u_o\right]\end{cases} \quad (7)$$

Where

$$G_h(s) = \frac{1-e^{-sT_s}}{sT_s} \quad (8)$$

$$G_i(z) = k_{\mathrm{p}} + k_{\mathrm{i}}\frac{T_s}{z-1} \quad (9)$$

$$z = e^{sT_s} \quad (10)$$

$$G_{\mathrm{PLL}}(z) = \frac{1}{2}\frac{H_{\mathrm{PI}}(z)\frac{T_s}{z-1}}{1+U_{\mathrm{m0}}H_{\mathrm{PI}}(z)\frac{T_s}{z-1}} \quad (11)$$

where $G_h(s)$ is the transfer function expression for the ZOH, $G_i(z)$ and $G_{\mathrm{PLL}}(z)$ are the discretized signals of the $G_i(s)$ and PLL, $H_{\mathrm{PI}}(\mathrm{z}) = k_{p-\mathrm{PLL}} + k_{i-\mathrm{PLL}}\frac{T_s}{(\mathrm{z}-1)}$, $k_{\text{p-pll}}$ and $k_{\text{i-pll}}$ are the proportional-integral (PI) coefficients of PLL.

Combining (7) and (11), it can be derived.

$$\Delta i_o = F(s)I_{\mathrm{m0}}G_{\mathrm{PLL}}(z)\Delta u_o^* - F(s)\Delta i_o^* - G_2(s)\Delta u_o \quad (12)$$

where $F(s) = G_2(s)G_1(s)G_h(s)z^{-1}K_{\mathrm{PWM}}G_{i\alpha\beta}(z)$

Discretizing both sides of (12) yields:

$$\Delta i_o^* = \frac{F^*(s)\,\mathrm{I_{m0}}\,G_{\mathrm{PLL}}(z)}{1+F^*(s)}\Delta u_o^* - \frac{\left(G_2(s)\Delta u_o\right)^*}{1+F^*(s)} \quad (13)$$

where $\Delta u_o^*(s)$ and $\Delta i_o^*(s)$ are the sampled voltage and sampled current, $F^*(s) = G_2(z)G_1(z)z^{-1}K_{\mathrm{PWM}}G_{i\alpha\beta}(z)$.

As the impedance model of GCI should represent the mathematical relationship between continuous voltage and continuous current, substituting (14) into (12), Δi_o is

$$\Delta i_o = \frac{F_s}{1+F^*(s)}\left[I_{\mathrm{m0}}G_{\mathrm{PLL}}(z)\Delta u_o^* + \left(G_2(s)\Delta u_o\right)^*\right] - G_2(s)\Delta u_o \quad (14)$$

Utilizing Poisson's sum formula on (14) and then simplifying, it can be obtained that

$$\Delta i_o = \frac{F(s)\,\mathrm{I_{m0}}\,G_{\mathrm{PLL}}(z)}{1+F^*(s)}\Delta u_o - \frac{G_2(s)(1+F^*(s)-F(s))}{1+F^*(s)}\Delta u_o \quad (15)$$

Based on (15) and Figure 6, similarly the Norton equivalent hybrid small-signal circuit of the GCI system can be described in Figure 7.

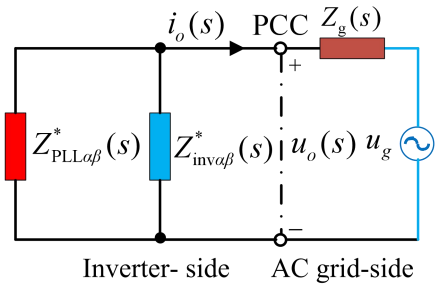

Figure 7. Norton equivalent mixed small-signal circuit of GCI in the $\alpha\beta$ domain

From Figure 7, it can be obtained:

$$Z^*_{o\alpha\beta}(s) = \frac{1}{\frac{1}{Z^*_{\mathrm{PLL}\alpha\beta}(s)} + \frac{1}{Z^*_{\mathrm{inv}\alpha\beta}(s)}} \quad (16)$$

where $Z^{*\mathrm{PLL}}_{\alpha\beta}(s)$ and $Z^{*\mathrm{inv}}_{\alpha\beta}(s)$ are represented as follows, respectively.

$$\begin{cases}Z^*_{\mathrm{PLL}\alpha\beta}(s) = -\dfrac{1+F^*(s)}{F(s)I_{\mathrm{m0}}G_{\mathrm{PLL}}(z)} \\ Z^*_{\mathrm{inv}\alpha\beta}(s) = \dfrac{1+F^*(s)}{G_2(s)(1+F^*(s)-F(s))}\end{cases} \quad (17)$$

Then the stability of the GCI system can be ascertained by examining the phase margin (PM) associated [29,30] with the crossover frequency on the magnitude plots of $Z_g(s)$ and $Z^*_{o\alpha\beta}(s)$. In other words, if the phase margin is positive, the system is deemed stable.

3. Stability Assessment based on SISO Impedance Model

In this section, an examples of Figure 1 is used to demonstrate the application of the small-signal stability evaluation method based on the hybrid impedance model in $\alpha\beta$ domain, the related parameters are given Table 1. The calculation examples of the influence of two parameters are designed to comparative analysis based on hybrid impedance model in dq domain [13]: (1) the effect of grid impedance on GCI stability. (2) The effect of PLL bandwidth on GCI stability.

Table 1. The main parameters of GCI system

Parameters	Value
U_{dc}	700 V
P	14 kW
L_2	1 mH
R_d	2 Ω
C_f	10 μF
U_g	220 V
f_g	50 Hz
k_p/k_i	0.6/300
f_s	10Hz

A. The Effect of Grid Impedance

The drawn bode diagram of Z_g with Z^*_{odq} and $Z^{*o}_{\alpha\beta}$ based on two impedance models is shown in Figure 8, which Z^*_{odq} is output impedance of GCI based on hybrid *dq* -impedance model [13]. When L_g=10mH (SCR=3.28), f_{PLL}=104Hz, other parameters coincide with the initial system. The PM of GCI system is PM=2.1°>0 based on Z^*_{odq} and PM=4.9°>0 based on $Z^{*o}_{\alpha\beta}$, which indicate that the GCI system is stable.

In Figure 9, when L_g parameter is set to 11mH (SCR=2.99), the bandwidth of PLL remains unchanged, the PM of GCI system is 2.3°>0 based on hybrid *dq* -impedance model Z^*_{odq}, which indicates the system is stable. However, based on the $Z^{*o}_{\alpha\beta}$, the corresponding PM is -0.4°＜0 at the intersection frequency, which indicates the system is unstable. Therefore the GCI system based on hybrid $\alpha\beta$ -impedance has lower conservatism than based on hybrid *dq* -impedance.

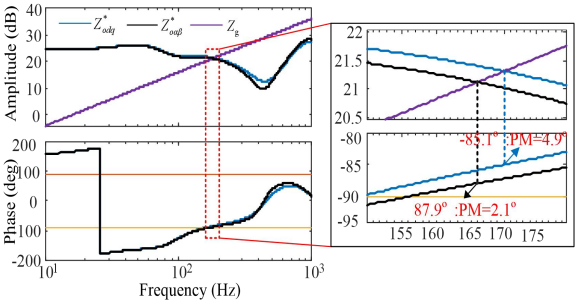

Figure 8. Stability analysis results under L_g=10mH (SCR=3.28), f_{PLL}=104Hz

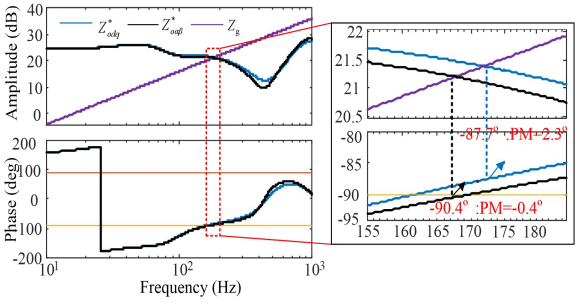

Figure 9. Stability analysis results L_g=11mH (SCR=2.99), f_{PLL}=104Hz

B. The Effect of PLL Bandwidth

Figure 10 displays the amplitude frequency characteristic curves of Z_g with Z^*_{odq} and $Z^{*o}_{\alpha\beta}$ based on two impedance models, respectively. When f_{PLL}=86Hz, L_g=12mH (SCR=2.74), other parameters coincide with the initial system. The PM of GCI system is PM=4.6°>0 based on $Z_{o\alpha\beta}$ and PM=1.8°>0 based on $Z^{*o}_{\alpha\beta}$, which indicate that the GCI system is stable.

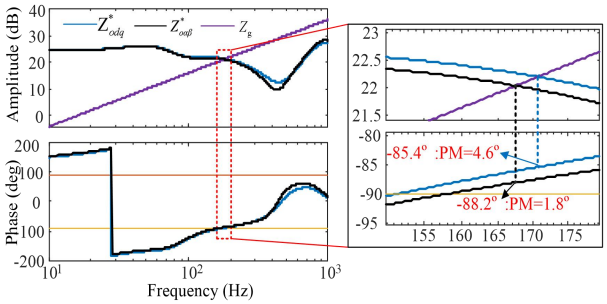

Figure 10. Stability analysis results under f_{PLL}=86Hz, L_g=12mH (SCR=2.74)

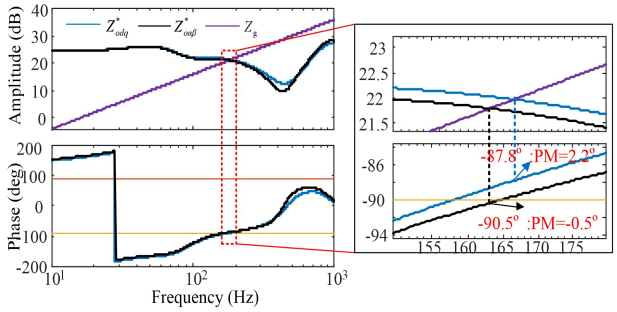

Figure 11. Stability analysis results f_{PLL}=95Hz, L_g=12mH (SCR=2.74)

In Figure 11, when the f_{PLL} parameter is set to 95Hz, the L_g parameter remains unchanged, the PM of GCI system is 2.2°>0 based on hybrid *dq* -impedance model Z^*_{odq}, which indicates the system is stable. However, based on the $Z^{*o}_{\alpha\beta}$, the corresponding PM=-0.5°＜0 at the intersection frequency, this suggests the system is unstable. Hence the GCI system based on hybrid $\alpha\beta$ -impedance has lower conservatism than based on hybrid *dq* -impedance.

C. Conservative Analysis

The following test can further compare the conservativeness of two impedance models. To get different cases, L_g is varied from 9 to 12, and the PLL bandwidth f_{PLL} is adjusted between [85,135]. The system stability is assessed based on impedance criterion for each case. Moreover, the corresponding security regions are also plotted which represents the set of parameters for stable GCI system operation. The results are displayed as the shadowed areas and boundary curve in Fig. 12. It can be seen that the stability region of the proposed hybrid impedance model is a subset of the continuous impedance model's stability region. Therefore, compared to the hybrid *dq* -

impedance model, the proposed hybrid $\alpha\beta$ -impedance model provides a more accurate assessment of system stability, making it more advantageous for guiding system parameter design.

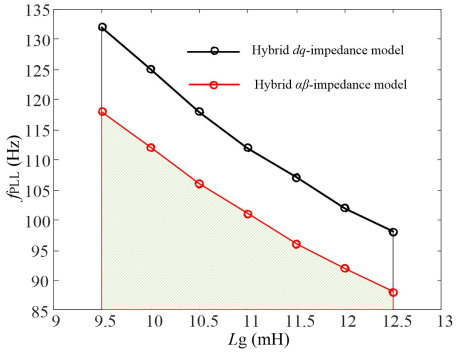

Figure 12. L_g - f_{PLL} stable region for two impedance models

4. Experimental Verification

In order to validate the correctness of the above theoretical analysis, a hardware-in-the-loop (HIL) testing setup for the 14kW GCI system has been constructed, as depicted in Figure 13. Experimental parameters are consistent with Table 1.

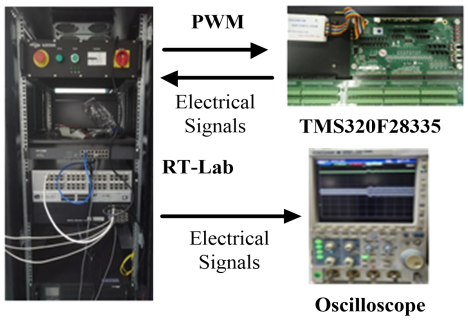

Figure13. Hardware-in-the-loop experimental platform

Figure 14 displays the time-domain waveform of voltage u_{oa} and grid-connected current i_{oabc} of GCI system. when L_g=10mH (SCR=3.28), f_{PLL}=104Hz, the GCI system is stable during half load and full load operation as shown Figure 14(a). The results are consistent with the stability analysis in Figure 8, which indicates the both impedance models built are correct. However, when L_g is set to 11mH, the system operates unstably during full load operation as shown Figure 14(b). In other words, the GCI system based on hybrid $\alpha\beta$ -impedance has lower conservatism than based on hybrid dq -impedance.

The same conclusions are evident by changing the parameter f_{PLL} of as well as shown Figure 15. When f_{PLL}=86Hz, L_g=12mH (SCR=2.74), the GCI system is stable during half load and full load operation as shown Figure 15(a). The results are consistent with the stability analysis in Figure 9, which indicates the stability analysis results based on both impedance models are correct. However, when f_{PLL} is set to 95Hz, the system operates unstably during full load operation as shown Figure 15(b). Having the same conclusion, the GCI system based on hybrid $\alpha\beta$ -impedance has lower conservatism than based on hybrid dq -impedance.

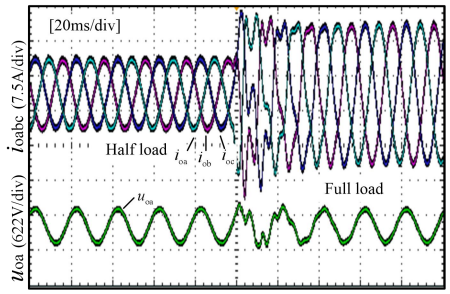

(a) L_g=10mH (SCR=3.28)

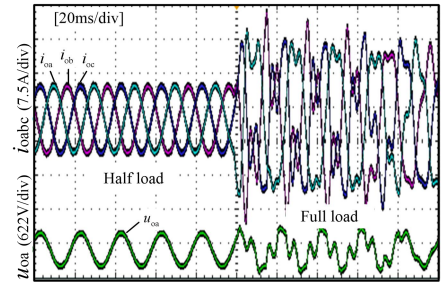

(b) L_g=11mH (SCR=2.99)

Figure 14. Experimental waveforms of GCI grid-connected currents under f_{PLL}=104Hz

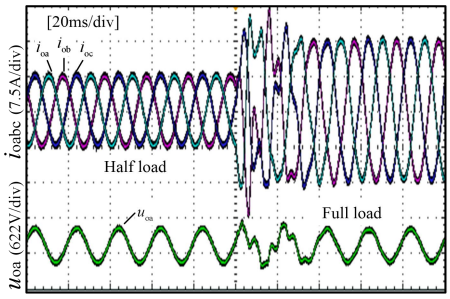

(a) f_{PLL}=86Hz

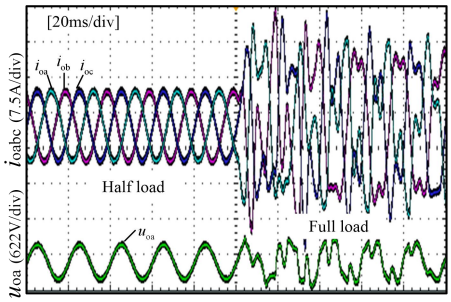

(b) f_{PLL}=95Hz

Figure 15. Experimental waveforms of GCI grid-connected currents under L_g=12mH (SCR=2.74)

5. Conclusion

In this paper, a SISO hybrid impedance model in $\alpha\beta$ domain is proposed to assess the small-signal stability of GCI system. The distinguished features of the article are as follows.

1) The proposed SISO hybrid impedance model is straightforward and intuitive for assessing the stability system margin, which is helpful to analysis stability of grid-connected systems.

2) Compared to the SISO hybrid dq -impedance model, The proposed SISO hybrid $\alpha\beta$ -impedance model has lower conservatism to assess the GCI stability, which can be more accurately identify the GCI system's oscillatory instability state.

Acknowledgment

Thank you for the support by the State Grid Corporation of China's industrial unit technology project, grant number DCHA-KJ-23290701.

References

[1] X.H. Wang, K. Qin, X.B. Ruan, D.H. Pan, Y.Y. He, et al. A robust grid-voltage feedforward scheme to improve adaptability of grid-connected inverter to weak grid condition. IEEE Transactions on Power Electronics. 2021, 36(2), 2384-2395. DOI: 10.1109/TPEL.2020.3008218

[2] R. Irnawan, R. Mochamad, F. Faria da Silva, Q. Zhang, S. Sarjiya, et al. Review of HVDC Technologies for Weak Grid Interconnectors. Electrical Engineering. 2024, 1-19. DOI: 10.1007/s00202-024-02761-6

[3] J.M. Xu, J.F. Zhong, J.H. Kang, W. Dong, S.J. Xie. Stability Analysis and Robust Parameter Design of DC-Voltage Loop for Three-Phase Grid-Connected PV Inverter Under Weak Grid Condition. IEEE Transactions on Industrial Electronics. 2024, 71(4), 3776-3787. DOI: 10.1109/TIE.2023.3277020

[4] X.F. Wang, F. Blaabjerg. Harmonic stability in power electronic-based power systems: Concept, modeling, and analysis. IEEE Transactions on Smart Grid. 2019, 10(3), 2858–2870. DOI: 10.1109/TSG.2018.2812712

[5] X.G. Zhang, S.D. Fu, W.J. Chen, N.N. Zhao, G.L. Wang, et al. A symmetrical control method for grid-connected converters to suppress the frequency coupling under weak grid conditions. IEEE Transactions on Power Electronics. 2020, 35(12), 13488–13499. DOI: 10.1109/TPEL.2020.2991185

[6] Z.H. Lin, X.B. Ruan, L.G. Wu, H. Zhang, W.W. Li. Multi resonant component based grid-voltage-weighted feed forward scheme for grid-connected inverter to suppress the injected grid current harmonics under weak grid. IEEE Transactions on Power Electronics. 2020, 35(9), 9784–9793. DOI: 10.1109/TPEL.2020.2970514

[7] B. Hu, H. Nian, M. Li, Y.Y. Xu, Y.M. Liao, et al. Impedance-based analysis and stability improvement of DFIG system within PLL bandwidth. IEEE Transactions on Industrial Electronics. 2022, 69(6), 5803-5814. DOI: 10.1016/j.ijepes.2020.105897

[8] G. Grdenić, M. Delimar, J. Beerten. Assessment of AC network modeling impact on small-signal stability of AC systems with VSC HVDC converters. International Journal of Electrical Power & Energy Systems. 2020, 119, 105897. DOI: 10.1016/j.ijepes.2020.105897

[9] E.S. Zhao, Y. Han, X.Y. Lin, P. Yang, F. Blaabjerg, et al. Impedance characteristics investigation and oscillation stability analysis for two-stage PV inverter under weak grid condition. Electric Power Systems Research. 2022, 209, 108053. DOI: 10.1016/j.epsr.2022.108053

[10] Z.W. Zeng, J.B. Zhao, Z.X. Liu, L. Mao, K.Q. Qu. Stability assessment and parametric sensitivity analysis based on extended Gershgorin theorem for multiple grid connected converters. Electric Power Systems Research. 2023, 214, 108913. DOI: 10.1016/j.epsr.2022.108913

[11] B. Wen, D. Boroyevich, R. Burgos, P. Mattavelli, Z.Y. Shen. Analysis of D-Q small-signal impedance of grid-tied inverters. IEEE Transactions on Power Electronics. 2016, 31(1), 675–687. DOI: 10.1109/TPEL.2015.2398192

[12] M. Cespedes, J. Sun. Impedance modeling and analysis of grid-connected voltage-source converters. IEEE Transactions on Power Electronics. 2014, 29(3), 1254-1261. DOI: 10.1109/TPEL.2013.2262473

[13] L.B. Huang, H.H. Xin, Z.Y. Li, P. Ju, H. Yuan, et al. Grid-synchronization stability analysis and loop shaping for PLL-based power converters with different reactive power control. IEEE Transactions on Smart Grid. 2020, 11(1), 501–516. DOI: 10.1109/TSG.2019.2924295

[14] A.D. Liu, J. Liu. Stability analysis and improved control of voltage source converters based on impedance models in weak grids. Electrical Engineering. 2024. DOI: 10.1007/s00202-024-02300-3

[15] J.Z. Shi, L.H. Yang, H. Yang, J.Q. Ji, Z.Y. Chen. Impedance modeling and quantitative stability analysis of grid - connected voltage source converters under complex unbalanced conditions. Electric Power Systems Research. 2025, 238, 111084. DOI: 10.1016/j.epsr.2024.111084

[16] Z.W. Xie, Y.D. Chen, W.H. Wu, W.L. Gong, L.M. Zhou, et al. Admittance modeling and stability analysis of grid-connected inverter with LADRC-PLL. IEEE Transactions on Industrial Electronics. 2021, 68(12), 12272-12284. DOI: 10.1109/TIE.2020.3044789

[17] E.S. Zhao, Y. Han, X.Y. Lin, E.P. Liu, P. Yang, et al. Harmonic characteristics and control strategies of grid - connected photovoltaic inverters under weak grid conditions. International Journal of Electrical Power & Energy Systems. 2022, 142, 108280. DOI: 10.1016/j.ijepes.2022.108280

[18] Y. Zhang, M.Q. Tian, H. Zhang, J.C. Song, W.J. Zhang. Admittance modeling and stability enhancement of grid - connected inverter considering frequency coupling in weak grids. Electric Power Systems Research. 2022, 209, 108034. DOI: 10.1016/j.epsr.2022.108034

[19] C.M. Tu, J.Y. Gao, F. Xiao, Q. Guo, F. Jiang. Stability Analysis of the Grid-Connected Inverter Considering the Asymmetric Positive-Feedback Loops Introduced by the PLL in Weak Grids. IEEE Transactions on Industrial Electronics. 2022, 69(6), 5793-5802. DOI: 10.1109/TIE.2021.3086716

[20] B.C. Shi, Z.M. Zhao, Y.C. Zhu, Z.J. Yu, J.H. Ju. A numerical convex lens for the state discretized modeling and simulation of megawatt power electronics systems as generalized hybrid systems. Engineering. 2021, 7(12), 1766–1777. DOI: 10.1016/j.eng.2021.07.011

[21] V. Pirsto, J. Kukkola, M. Hinkkanen, L. Harnefors. Intersample modeling of the converter output admittance. IEEE Transactions on Industrial Electronics. 2021, 68(11), 11348-11358. DOI: 10.1109/TIE.2020.3029482

[22] F.D. Freijedo, M. Ferrer, D. Dujic. Multivariable high frequency input-admittance of grid-connected converters: Modeling, validation, and implications on stability. IEEE Transactions on Industrial Electronics. 2019, 66(8), 6505-6515. DOI: 10.1109/TIE.2019.2892701

[23] E. Rodriguez-Diaz, F.D. Freijedo, J.M. Guerrero, J.A. Marrero-Sosa, D. Dujic, et al. Input-admittance passivity compliance for grid-connected converters with an LCL filter. IEEE Transactions on Industrial Electronics. 2019, 66(2), 1089-1097. DOI: 10.1109/TIE.2018.2835374

[24] M.B. Araujo, R.P. Vieira. Discrete-time backstepping-state feedback approach for current control of LCL grid-tied converters. International Journal of Electrical Power & Energy Systems. 2021, 133, 107220. DOI: 10.1016/j.ijepes.2021.107220

[25] W.B. Wu, K. Hu, M. Zhang, G.J. Han. Fully discrete-time domain model and damping characteristics accurate analysis for grid-connected inverter with LCL filter. Electric Power Systems Research. 2023, 221, 109388. DOI: 10.1016/j.epsr.2023.109388

[26] J. Bu, Q. Li, Q. Li, Z.Y. Chen, Y.C. Huo, et al. Inertia compensation for wind turbine emulator based on anticipation deviation suppression. Electric Power Systems Research. 2023, 224, 109751. DOI: 10.1016/j.epsr.2023.109751

[27] Y.J. Zhu, J.B. Zhao, Z.W. Zeng, L. Mao, K.Q. Qu. SISO impedance modeling and stability comparison of grid-connected inverter control system in different time domains. Electric Power Systems Research. 2024, 228, 110069. DOI: 10.1016/j.epsr.2023.110069

[28] M.Z. Zhu, J.Q. Liu, L.J. Chen, L. Ge. Stability-Improved Repetitive Control for Inverters Considering PLLs Under Weak Grid Conditions. Journal of Power Electronics. 2024. DOI: 10.1007/s43236-024-00925-y

[29] H.L. Zhu, Z.Q. Zhang, L. Fickert, G.C. Chen, Y.M. Zhang, et al. Impedance Measurement and Stability Analysis Based on Grid-Connected Inverter in D-Q Domain. 24th International Scientific Conference on Electric Power Engineering (EPE), Kouty nad Desnou, Czech Republic. 2024, 285-288. DOI: 10.1109/EPE61521.2024.10559505

[30] G.X. Li, H.Z. Pan, X. Liu, L.F. Yin, H.H. Goh. PLL Phase Margin Design and Analysis for Mitigating Sub/Super-Synchronous Oscillation of Grid-Connected Inverter Under Weak Grid. International Journal of Electrical Power & Energy Systems. 2023, 151, 109124. DOI: 10.1016/j.ijepes.2023.109124